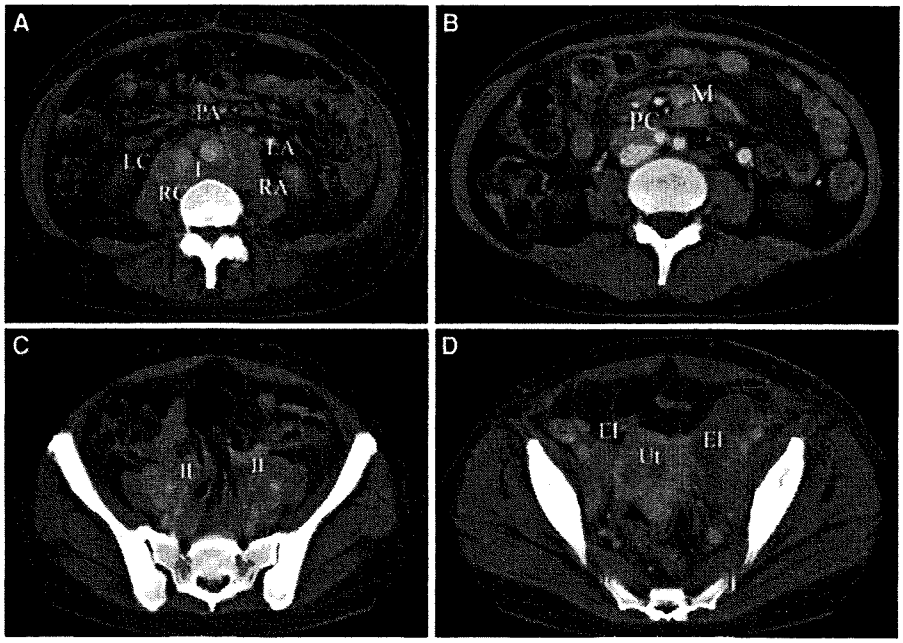

Fig. 1. A–D Axial contrast-enhanced CT image shows multiple enlarged lymph nodes in patient with follicular lymphoma. LA, lateroaortic lymph node; PA, preaortic lymph node; RA, retroaortic lymph node; LC, laterocaval lymph node; PC, precaval lymph node; RC, retrocaval lymph node; I, intermediate lumbar lymph node; M, mesenteric lymph node; II, internal iliac lymph node; EI, external iliac lymph node; Ut, uterus.

Imaging

The extent of disease does not necessarily correlate with the degree of ^{18}FDG accumulation; that is, some patients with ^{18}FDG-avid lymphoma show aggressive nature, whereas others with little avidity in the face of normal ^{18}FDG PET/CT may have systemic disease. Contrast-enhanced CT and ^{18}FDG PET have been sensitive for the detection of disease extent. However, contrast-enhanced CT and ^{18}FDG PET/CT are more sensitive and specific and are utilized for staging prior to therapy, re-staging after therapy or detection of recurrent disease, and the early recognition of therapeutic effect and clinical outcome [17–20].

Conventional CT

Conventional whole-body CT is routinely used for detection of lymphadenopathy. It is more preferable with a scan delay set at nearly 60 s after intravenous injection of contrast media. Although the detectability of lesions depends on slice thickness of standard reconstructed images which mostly ranges from 5.0 to 10.0 mm by means of a standard algorithm, nonmutually exclusive findings of lymphadenopathy may be seen: (1) enlarged lymph node greater than 10.0 mm in the axial plane and (2) enlarged lymph node with enhancement and its degree is greater than those of muscle and less than those of vessels (Fig. 1). Moreover, if an involved node is not enlarged greater than 10.0 mm, CT images may not reveal enough densities, especially when standard 7.0- or 10.0-mm-thick images are obtained. Conventional whole-body CT is performed prior to treatment and follow-up after treatment with a follow-up period usually at least every 3 or 6 months.

PET/CT

Because small involved lymph nodes are often misinterpreted as reactive lymph nodes on CT, ^{18}FDG PET/CT helps sort out equivocal cases. Generally, initial PET/CT is performed before therapy. Scans were acquired with PET/CT device that consisted of a PET scanner which had the theoretical spatial resolution and multislice CT scanner with a whole-body mode implemented as the standard software. Prior to the PET/CT study, the patients were fasted for at least 6 h. All patients were tested for a normal glucose level (range, 80–120 mg/dl) before ^{18}FDG administration. At first, noncontrasted CT for attenuation correction was performed from the head to the mid-thigh according to a standardized protocol with the following setting. Emission scans from the base of the skull to the mid-thigh were then obtained at about 60 min after the intravenous administration of ^{18}FDG.

Noncontrasted PET/CT can improve accuracy of staging compared with PET alone or diagnostic contrast-enhanced CT alone in patients with malignant lymphoma. However, the use of intravascular contrast material has an additional diagnostic impact in nodal staging of malignant lymphoma. After PET acquisition of 2–5 min per table position, contrast-enhanced CT was performed for the purpose of contrast-enhanced PET/CT from the head to the mid-thigh according to the same protocol as those

of CT without contrast enhancement. A total of 100 ml contrast material is administered intravenously using an autoinjector with a rate of 2.0 ml/s. Scan delay is set at 50–60 s after injection of contrast media [21–23].

Anatomic distribution of pelvic and retroperitoneal lymph nodes

The lymphatic pathway of pelvic organs drains either to visceral lymph nodes or regional nodes. The iliac lymph nodes consist of three different chains: right or left medial, intermediate, and right or left lateral (Table 1). The main channel which is often observed in iliac lymph nodes depends on nodal station and accompanying blood vessels. The main channel of the common iliac lymph node is the lateral chain. However, the main channel of the internal or external iliac lymph node is the medial chain. Recognition of the main channel in each lymph node is important for staging diagnosis because lymph nodes of the main channel are mostly involved in malignant lymphoma.

Retroperitoneal lymphatic pathway possesses different drainage areas from intraperitoneal lymphatic pathway. Retroperitoneal lymph nodes drain mainly to the lumbar lymph nodes, e.g., retrocaval lymph nodes, precaval lymph nodes, laterocaval lymph nodes, and intermediate lumbar lymph nodes (Table 1). The efferent lymph vessels from lumbar lymph nodes link to the thoracic duct together with the intestinal lymphatic trunk which includes mesenteric lymph nodes draining small and large intestine and the pelvic chain.

Table 1. Lymphatic pathway adjacent to urinary tract

Lymph node station	Laterality	
Lumbar lymph node		
Retrocaval lymph node	Rt	Lt
Precaval lymph node	NA	
Laterocaval lymph node	Rt	
Intermediate lumbar lymph node	NA	
Retroaortic lymph node	Rt	Lt
Preaortic lymph node	Rt	Lt
Lateroaortic lymph node		Lt
Pelvic lymph node		
Common iliac lateral lymph node	Rt	Lt
Common iliac intermediate lymph node	NA	
Common iliac promontory lymph node	NA	
Sigmoid lymph node[a]		Lt
Juxtaintestinal lymph node[a]		Lt
Internal iliac lymph node	Rt	Lt
External iliac lymph node	Rt	Lt
Pararectal lymph node[a]	Rt	Lt
Laterovesical lymph node[a]	Rt	Lt
Retrovesical lymph node[a]	Rt	Lt
Parauterine lymph node[a]	Rt	Lt

[a]Rarely involved lymph nodes
NA, not available; Rt, right; Lt, left

Abnormal uptake in the pelvic and retroperitoneal lymph nodes

At the initial staging, the pelvic and retroperitoneal lymph nodes are mostly involved in patients with Hodgkin lymphoma and non-Hodgkin's lymphoma: follicular lymphoma, diffuse large B-cell lymphoma, marginal zone B-cell lymphoma of mucosa-associated lymphoid tissue (MALT) type, and mantle cell lymphoma [24–26]. Intensely increased, partially symmetric ^{18}FDG accumulation is noted in the areas of the pelvic and retroperitoneal lymphatic pathway correlating to areas of lymphadenopathy on CT. Lumbar lymph nodes including the retrocaval lymph node, intermediate lumbar lymph node, retroaortic lymph node, and lateroaortic lymph node are most frequently involved at the initial presentation (Fig. 2). Abnormal uptake is often significant continuously from the precaval or preaortic lymph nodes to superior mesenteric lymph nodes, pancreaticoduodenal lymph nodes, and juxtaintestinal lymph nodes in patients with follicular lymphoma of various grades (Fig. 3). The lateral and intermediate common iliac lymph nodes, internal lilac lymph nodes, and external iliac lymph nodes are mostly involved in any types of malignant lymphoma (Fig. 4). However, lymph nodes of the common iliac promontory are frequently involved in follicular lymphoma (Fig. 5). On the other hand, areas of increased tracer activity often do not correlate to any mass lesions on CT. These areas of uptake represent normal physiological variants: urinary and intestinal activity or anatomic variants. Focal uptake of the ureter presenting at the lateral common iliac area mimics nodal involvement (Fig. 6). Normal activity in the jejunum is often misinterpreted as abnormal uptake in the external iliac lymph nodes (Fig. 7).

Differentiation of abnormal uptake from normal physiological variants with contrast-enhanced PET/CT

Integrated contrast-enhanced PET/CT improves the diagnostic accuracy in evaluating nodal status of pelvic and retroperitoneal lymphatic pathways in patients with malignant lymphoma, particularly detects a nodal involvement in a group of iliac lymph nodes adjacent to the ureter. Morimoto and colleagues described 66 patients with malignant lymphoma who underwent both noncontrasted PET/CT and contrast-enhanced PET/CT [21]. Nodal stage of pelvic and retroperitoneal lymphatic pathways was correctly determined in 47 patients on noncontrasted PET/CT, whereas determination of lymph node involvement based on contrast-enhanced PET/CT was correctly staged in 52 patients. Difference in the accuracy of nodal status between noncontrasted PET/CT and contrast-enhanced PET/CT was significant by McNemar test (Fig. 8).

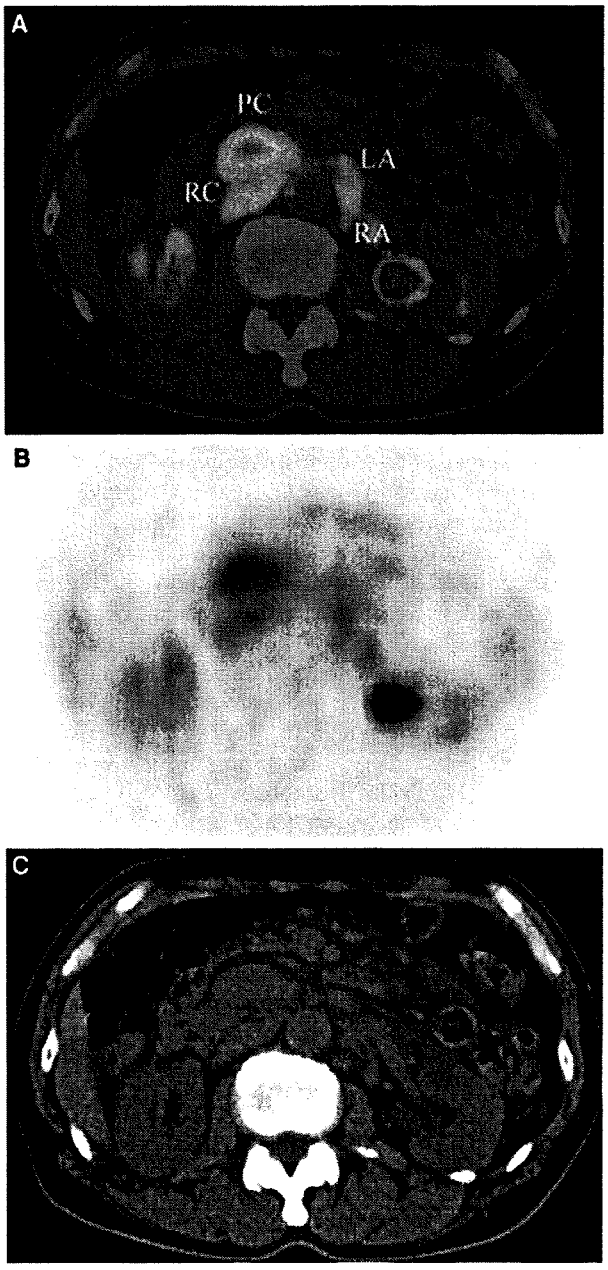

Fig. 2. Axial noncontrasted PET/CT image (A), PET (B), and CT (C) shows multiple enlarged nodes with increased uptake in patient with follicular lymphoma. LA, lateroaortic lymph node; RA, retroaortic lymph node; PC, precaval lymph node; RC, retrocaval lymph node.

Contrast-enhanced PET/CT determines the status of the common iliac lymph node, internal iliac lymph node, and external iliac lymph node more accurately than PET/CT. False-positive findings on contrast-enhanced PET/CT may be caused by misdiagnosing ureters or intestinal

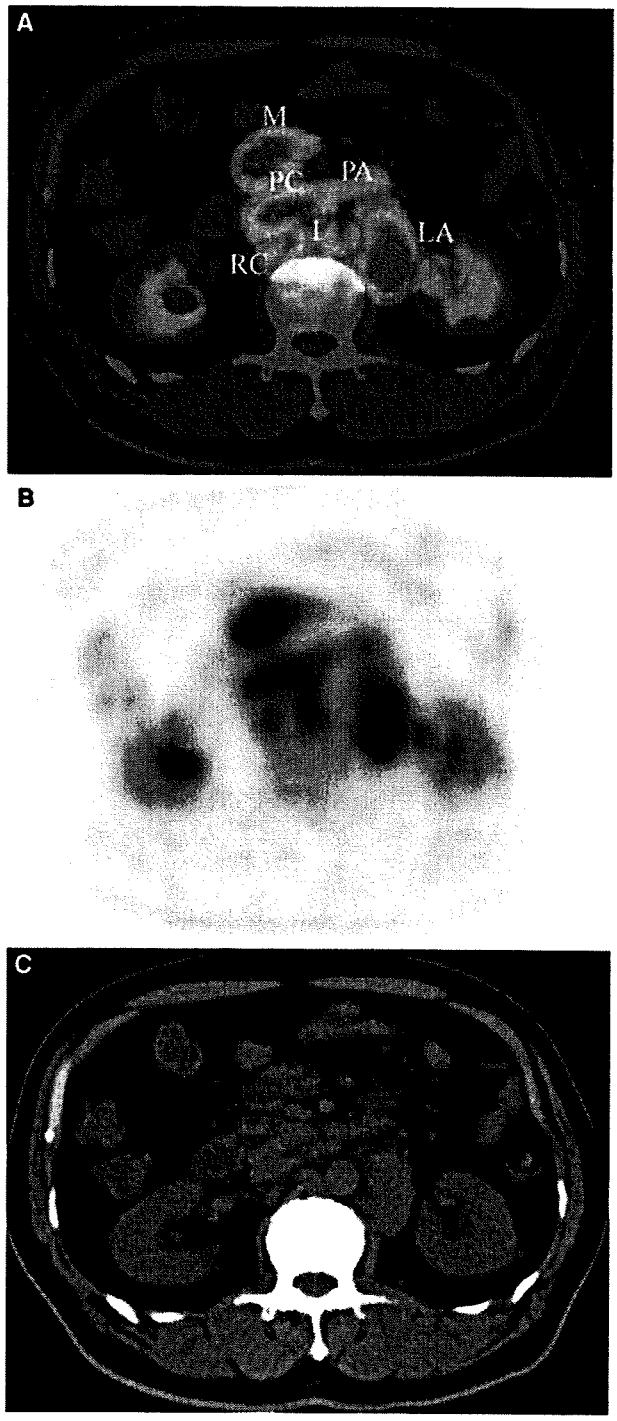

Fig. 3. Axial noncontrasted PET/CT image (A), PET (B), and CT (C) shows multiple enlarged nodes with increased uptake in patient with follicular lymphoma. LA, lateroaortic lymph node; PA, preaortic lymph node; PC, precaval lymph node; I, intermediate lumbar lymph node; RC, retrocaval lymph node; M, mesenteric lymph node.

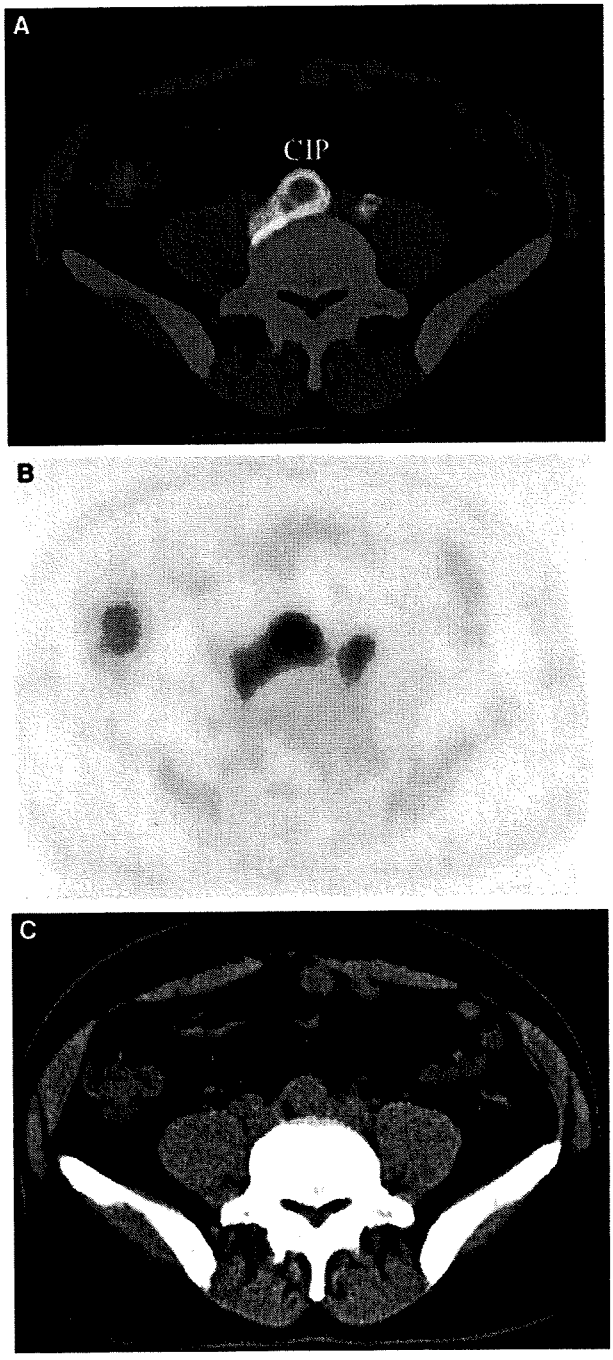

Fig. 4. Axial noncontrasted PET/CT image (**A**), PET (**B**), and CT (**C**) shows enlarged common iliac promontory (CIP) lymph nodes with increased uptake in patient with follicular lymphoma.

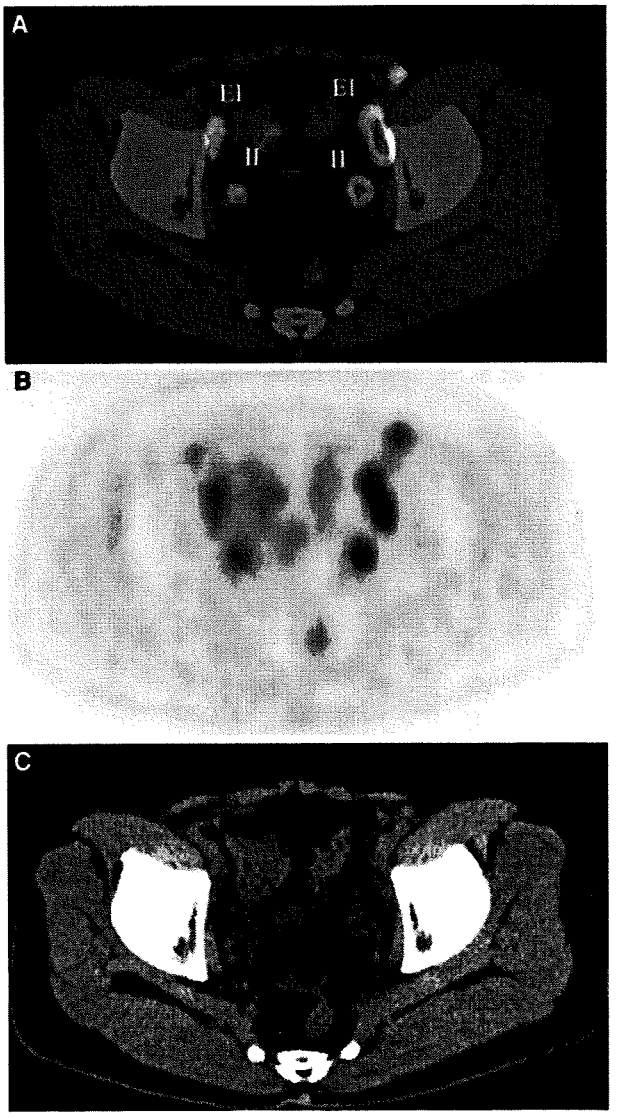

Fig. 5. Axial noncontrasted PET/CT image (**A**), PET (**B**), and CT (**C**) shows multiple enlarged nodes with increased uptake in patient with follicular lymphoma. **II**, internal iliac lymph node and **EI**, external iliac lymph node.

^{18}FDG uptake as lymph nodes. False-negative findings on contrast-enhanced PET/CT will be mainly due to involvement of subcentimeteric lymph nodes. However, diagnostic accuracies of lumbar lymph nodes: preaortic, lateroaortic, retroaortic, precaval, laterocaval, retrocaval, and intermediate lumbar nodes are similar by either noncontrasted PET/CT or contrast-enhanced PET/CT (Fig. 9). False-positive results in these nodes are often caused by misdiagnosing ureters as lymph nodes on both PET/CT with and without contrast enhancement. False-negative results of paraaortic and aortocaval lymph nodes are caused by intestinal ^{18}FDG uptake.

Clinical advantage by contrast-enhanced PET/CT

The lymphatic chains of the retroperitoneum and pelvis are complicated and numerous. Lymph nodes along the

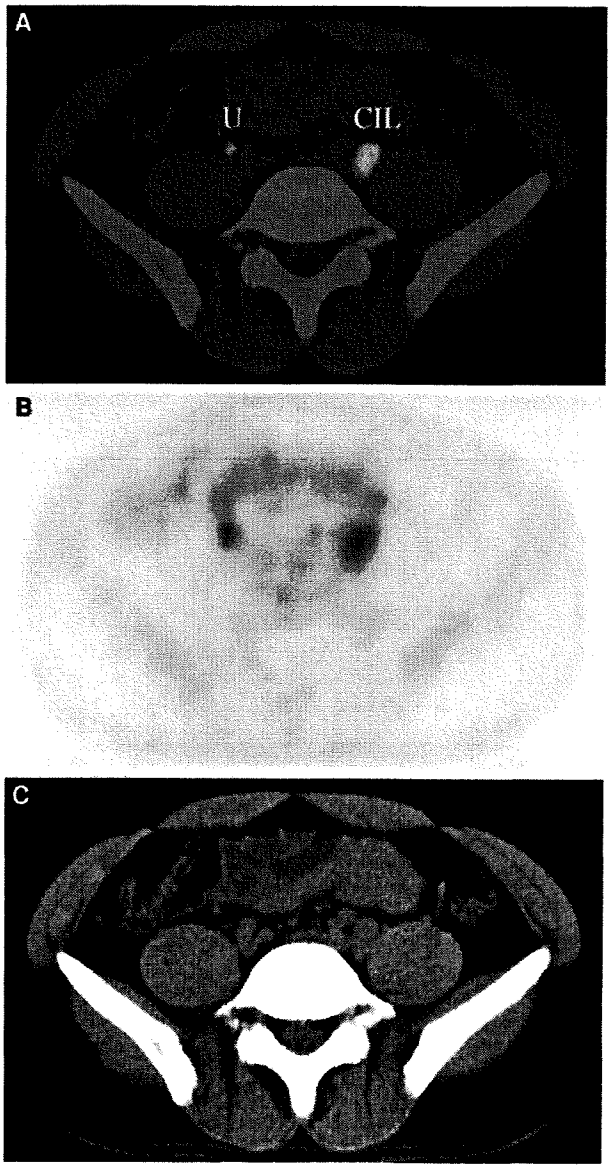

Fig. 6. Axial noncontrasted PET/CT image (**A**), PET (**B**), and CT (**C**) shows enlarged common iliac lateral lymph nodes with increased uptake in patient with follicular lymphoma. Focal uptake of ureter mimics abnormal uptake of common iliac lateral lymph node. CIL, common iliac lateral lymph node and U, ureter.

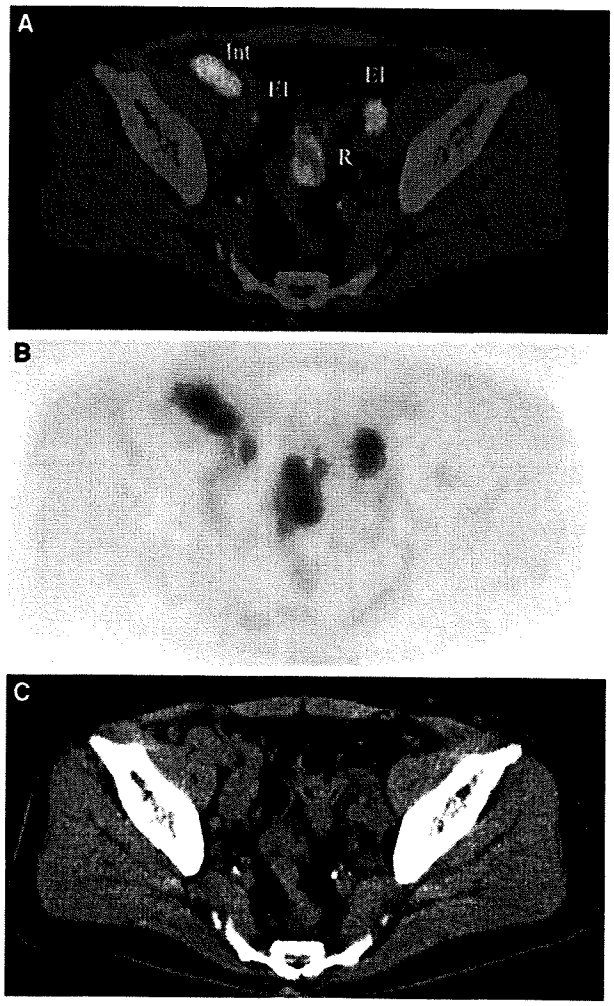

Fig. 7. Axial noncontrasted PET/CT image (**A**), PET (**B**), and CT (**C**) shows multiple enlarged nodes with increased uptake in patient with follicular lymphoma. Focal uptake of intestine (Int) mimics abnormal uptake of external iliac lateral lymph node. EI, external iliac lymph node and R, rectum.

pelvic and retroperitoneal lymphatic pathways are often identified at the initial presentation in patients with malignant lymphoma [27]. However, precise localization of lymph nodes in these regions is difficult only by noncontrasted images except for a bulky lesion. Contrast-enhanced PET/CT can reduce overstaged patients in number compared with noncontrasted PET/CT. In contrast, clinical stage will change from stage I or II to stage IV in patients who have a single focus along the pelvic and retroperitoneal lymphatic pathways. In addition, contrast-enhanced PET/CT depicts intravascular extension of tumor that cannot be diagnosed with noncontrasted PET/CT (Fig. 10). A recent study reported additional value of contrast-enhanced PET/CT compared with noncontrasted PET/CT in 47 patients with malignant lymphoma [23]. Diagnostic performance of two modalities is similar for initial staging with perfect correlation by Kappa statistics. However, unsuspected endometrial carcinoma and jugular thrombosis were identified only by contrast-enhanced PET/CT. Incidental findings, which often affect clinical outcome, will be observed by contrast-enhanced PET/CT.

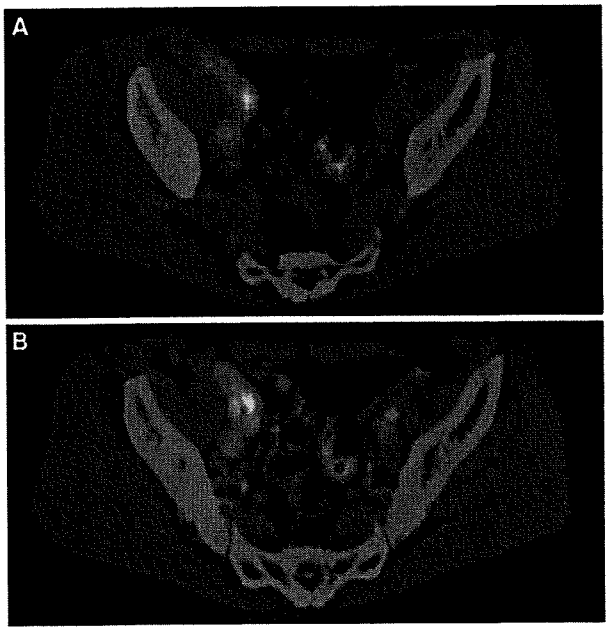

Fig. 8. Axial noncontrasted PET/CT image (**A**) and contrast-enhanced PET/CT (**B**) shows enlarged right internal iliac lymph node with increased uptake in patient with follicular lymphoma. Abnormal uptake is found in the right external iliac area on noncontrasted PET/CT, while this uptake corresponds to physiological uptake of jejunum on contrast-enhanced PET/CT.

Fig. 9. Axial noncontrasted PET/CT image (**A**) and contrast-enhanced PET/CT (**B**) shows multiple enlarged lumbar lymph nodes with increased uptake in patient with follicular lymphoma. Delineation of the lesion is better on contrast-enhanced PET/CT.

Direct comparison of noncontrasted PET/CT and contrast-enhanced PET/CT

The advantage of using contrast-enhanced PET/CT is due to more accurate determination of lymph nodes along pelvic and retroperitoneal lymphatic pathways. Compared with noncontrasted PET/CT, contrast-enhanced PET/CT enabled more accurate staging, which results in an altered therapeutic plan. However, the diagnostic performance of PET/CT should be elucidated compared with standard contrast-enhanced CT in staging of malignant lymphoma. Tatsumi and colleagues performed a comparative study of PET and CT portion derived from PET/CT in 53 patients with malignant lymphoma [28]. Positive lesions identified by both modalities were mostly concordant by three physicians. However, 17% of 1,537 anatomic sites had discordant findings between PET and CT, and most of these lesions were truly positive by PET alone. The exact role of PET/CT in identification of a lesion will be provided by the PET portion of PET/CT which can differentiate undetermined lesions on CT. In contrast, Schaefer and colleagues conducted a prospective study comparing diagnostic accuracy between noncontrasted PET/CT and contrast-enhanced CT in 60 patients with malignant lymphoma [29]. Although diagnostic accuracies are different for evaluation of nodal or extranodal disease status, noncontrasted PET/CT is more accurate than contrast-enhanced CT in patients with malignant lymphoma. The study suggests that routine noncontrasted PET/CT should be performed at staging or restaging in malignant lymphoma instead of contrast-enhanced CT.

Influences of contrast agents on standardized uptake value (SUV)

Significant improvements in evaluating nodal status of pelvic and retroperitoneal lymphatic pathways are found with contrast-enhanced PET/CT. However, it should be clarified whether contrast media can affect SUV of the lesion in patients with malignant lymphoma. Vera and colleagues investigated quantitative evaluation of SUV on contrast-enhanced PET/CT in 50 patients with malignant lymphoma [22]. They found limited change of SUV (maximum 4%) on contrast-enhanced PET/CT compared with noncontrasted PET/CT before therapy and little change of SUV after therapy. Their results will

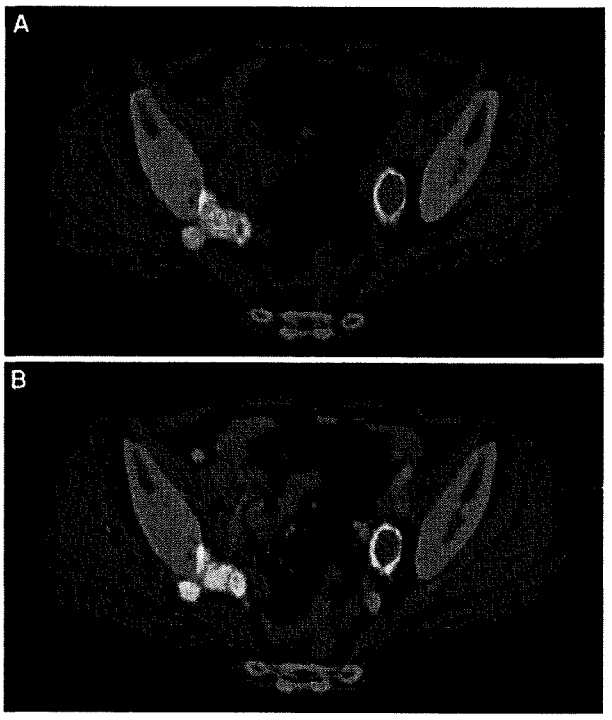

Fig. 10. Axial noncontrasted PET/CT image (**A**) and contrast-enhanced PET/CT (**B**) shows enlarged nodes with increased uptake in patient with follicular lymphoma. Abnormal uptake is found in the right gluteal lesion. Disappearance of right upper gluteal artery, which reflects intravascular extension, is also seen on contrast-enhanced PET/CT. Intense uptake is observed in the left hydroureter.

suggest that the difference of PET measurements by contrast-enhanced PET/CT is negligible and routine use of contrast-enhanced PET/CT is preferred for staging and follow-up in patients with malignant lymphoma.

Limitations

Despite the fact that noncontrasted or contrast-enhanced PET/CT improves the accuracy in staging or restaging in malignant lymphoma, the spatial resolution of PET/CT is not sufficient to detect small lymph nodes [30–32]. False-negative results are mainly due to small true-positive lymph nodes which are missed by PET/CT [18, 33–35]. On the other hand, main false-positive results are caused by misdiagnosis of physiological ^{18}FDG uptake as lymph node involvement. In the pelvic and retroperitoneal lymphatic pathways, urinary ^{18}FDG uptake often masks adjacent adenopathy by artifacts and makes lymph nodes less conspicuous [30–32]. A focal area of urinary uptake in ureter can also simulate nodal involvement. The proximal ureter parallels central retroperitoneal lymphatics and the distal third of the ureter lies in the extraperitoneal pelvis. The normal intestine commonly causes increased uptake of ^{18}FDG. Possible causes of ^{18}FDG uptake in the digestive tract are active smooth muscle, metabolically active mucosa, swallowed secretion, and colonic microbial uptake [30–32]. Intense FDG activity of the intestine can appear larger on PET/CT images than the actual size of the tracer collection. This phenomenon can affect assessment of retroperitoneal and pelvic lymph nodes.

Pathological examination for evaluating nodal status of pelvic and retroperitoneal lymph nodes which may be a cause of biased comparison is not performed routinely in the clinical setting. The cost effectiveness of contrast-enhanced PET/CT has not been fully elucidated. The relation between the benefit obtained by contrast-enhanced PET/CT and the risk of radiation exposure needs to be taken into account. The benefit–risk relationship between contrast-enhanced PET/CT and noncontrasted PET/CT should be clarified.

Conclusion

Nodal involvement of pelvic and retroperitoneal lymphatic pathways is often observed in patients with several histologic types of malignant lymphoma. These include Hodgkin lymphoma, follicular lymphoma, diffuse large B-cell lymphoma, marginal zone B-cell lymphoma of MALT type, and mantle cell lymphoma. Current diagnostic studies may be useful in revealing nodal status for purpose of staging or re-staging after treatment. Contrast-enhanced CT and noncontrasted PET/CT can detect typical involvement of each nodal station. Contrast-enhanced PET/CT is superior to standard staging method in detecting nodal involvement in a group of pelvic and retroperitoneal lymphatic pathways when these conditions are clinically suspected.

Acknowledgments. This work was supported in part by grants from Scientific Research Expenses for Health and Welfare Programs and the Grant-in-Aid for Cancer Research from the Ministry of Health, Labour and Welfare.

References

1. Jhanwar YS, Straus DJ (2006) The role of PET in lymphoma. J Nucl Med 47:1326–1334
2. Isasi CR, Lu P, Blaufox MD (2005) A metaanalysis of 18F-2-deoxy-2-fluoro-D-glucose positron emission tomography in the staging and restaging of patients with lymphoma. Cancer 104:1066–1074
3. Hicks RJ, Mac Manus MP, Seymour JF (2005) Initial staging of lymphoma with positron emission tomography and computed tomography. Semin Nucl Med 35:165–175
4. Podoloff DA, Macapinlac HA (2007) PET and PET/CT in management of the lymphomas. Radiol Clin North Am 45:689–696
5. Kumar R, Maillard I, Schuster SJ, Alavi A (2004) Utility of fluorodeoxyglucose-PET imaging in the management of patients with Hodgkin's and non-Hodgkin's lymphomas. Radiol Clin North Am 42:1083–1100
6. Burton C, Ell P, Linch D (2004) The role of PET imaging in lymphoma. Br J Haematol 126:772–784
7. Ulaner GA, Colletti PM, Conti PS (2008) B-cell non-Hodgkin lymphoma: PET/CT evaluation after 90Y-ibritumomab tiuxetan radioimmunotherapy—initial experience. Radiology 246:895–902

8. Hutchings M, Loft A, Hansen M, et al. (2006) FDG-PET after two cycles of chemotherapy predicts treatment failure and progression-free survival in Hodgkin lymphoma. Blood 107:52–59
9. Beal KP, Yeung HW, Yahalom J (2005) FDG-PET scanning for detection and staging of extranodal marginal zone lymphomas of the MALT type: a report of 42 cases. Ann Oncol 16:473–480
10. Karam M, Novak L, Cyriac J, et al. (2006) Role of fluorine-18 fluoro-deoxyglucose positron emission tomography scan in the evaluation and follow-up of patients with low-grade lymphomas. Cancer 107:175–183
11. Kumar R, Xiu Y, Zhuang HM, Alavi A (2006) 18F-fluorodeoxyglucose-positron emission tomography in evaluation of primary cutaneous lymphoma. Br J Dermatol 155:357–363
12. Tsai EY, Taur A, Espinosa L, et al. (2006) Staging accuracy in mycosis fungoides and sezary syndrome using integrated positron emission tomography and computed tomography. Arch Dermatol 142:577–584
13. Wohrer S, Jaeger U, Kletter K, et al. (2006) 18F-fluoro-deoxyglucose positron emission tomography (18F-FDG-PET) visualizes follicular lymphoma irrespective of grading. Ann Oncol 17:780–784
14. Ghersin E, Keidar Z, Eldad DJ, et al. (2007) Multimodality imaging of direct ureteric involvement in non-Hodgkin's lymphoma using PET/CT, CT urography and antegrade CT pyelography. Br J Radiol 80:e283–e286
15. Abouzied MM, Crawford ES, Nabi HA (2005) 18F-FDG imaging: pitfalls and artifacts. J Nucl Med Technol 33:145–155
16. Vesselle HJ, Miraldi FD (1998) FDG PET of the retroperitoneum: normal anatomy, variants, pathologic conditions, and strategies to avoid diagnostic pitfalls. Radiographics 18:805–823
17. von Schulthess GK, Steinert HC, Hany TF (2006) Integrated PET/CT: current applications and future directions. Radiology 238:405–422
18. Allen-Auerbach M, Quon A, Weber WA, et al. (2004) Comparison between 2-deoxy-2-[18F]fluoro-D-glucose positron emission tomography and positron emission tomography/computed tomography hardware fusion for staging of patients with lymphoma. Mol Imaging Biol 6:411–416
19. Freudenberg LS, Antoch G, Schutt P, et al. (2004) FDG-PET/CT in re-staging of patients with lymphoma. Eur J Nucl Med Mol Imaging 31:325–329
20. Raanani P, Shasha Y, Perry C, et al. (2006) Is CT scan still necessary for staging in Hodgkin and non-Hodgkin lymphoma patients in the PET/CT era? Ann Oncol 17:117–122
21. Morimoto T, Tateishi U, Maeda T, et al. (2007) Nodal status of malignant lymphoma in pelvic and retroperitoneal lymphatic pathways: comparison of integrated PET/CT with or without contrast enhancement. Eur J Radiol 67:508–513
22. Vera P, Ouvrier MJ, Hapdey S, et al. (2007) Does chemotherapy influence the quantification of SUV when contrast-enhanced CT is used in PET/CT in lymphoma? Eur J Nucl Med Mol Imaging 34:1943–1952
23. Rodríguez-Vigil B, Gómez-León N, Pinilla I, et al. (2006) PET/CT in lymphoma: prospective study of enhanced full-dose PET/CT versus unenhanced low-dose PET/CT. J Nucl Med 47:1643–1648
24. Even-Sapir E, Lievshitz G, Perry C, et al. (2007) Fluorine-18 fluorodeoxyglucose PET/CT patterns of extranodal involvement in patients with Non-Hodgkin lymphoma and Hodgkin's disease. Radiol Clin North Am 45:697–709
25. Bar-Shalom R (2007) Normal and abnormal patterns of 18F-fluorodeoxyglucose PET/CT in lymphoma. Radiol Clin North Am 45:677–688
26. Perry C, Herishanu Y, Metzer U, et al. (2007) Diagnostic accuracy of PET/CT in patients with extranodal marginal zone MALT lymphoma. Eur J Haematol 79:205–209
27. Macapinlac HA (2004) The utility of 2-deoxy-2-[18F]fluoro-D-glucose-positron emission tomography and combined positron emission tomography and computed tomography in lymphoma and melanoma. Mol Imaging Biol 6:200–207
28. Tatsumi M, Cohade C, Nakamoto Y, Fishman EK, Wahl RL (2005) Direct comparison of FDG PET and CT findings in patients with lymphoma: initial experience. Radiology 237:1038–1045
29. Schaefer NG, Taverna C, Strobel K, et al. (2007) Hodgkin disease: diagnostic value of FDG PET/CT after first-line therapy—is biopsy of FDG-avid lesions still needed? Radiology 244:257–262
30. Rodriguez-Vigil B, Gomez-Leon N, Pinilla I, et al. (2006) Positron emission tomography/computed tomography in the management of Hodgkin's disease and non-Hodgkin's lymphoma. Curr Probl Diagn Radiol 35:151–163
31. Strauss LG (1996) Fluorine-18 deoxyglucose and false-positive results: a major problem in the diagnostics of oncological patients. Eur J Nucl Med 23:1409–1415
32. Cook GJR, Fogelman I, Maisey MN (1996) Normal physiological and benign pathological variants of 18-fluoro-2-deoxyglucose positron emission tomography scanning: potential for error in interpretation. Semin Nucl Med 7:441–446
33. Hernandez-Maraver D, Hernandez-Navarro F, Gomez-Leon N, et al. (2006) Positron emission tomography/computed tomography: diagnostic accuracy in lymphoma. Br J Haematol 135:293–302
34. la Fougère C, Hundt W, Bröckel N, et al. (2006) Value of PET/CT versus PET and CT performed as separate investigations in patients with Hodgkin's disease and non-Hodgkin's lymphoma. Eur J Nucl Med Mol Imaging 33:1417–1425
35. Rhodes MM, Delbeke D, Whitlock JA, et al. (2006) Utility of FDG-PET/CT in follow-up of children treated for Hodgkin and non-Hodgkin lymphoma. J Pediatr Hematol Oncol 28:300–306

特集　リツキシマブ導入後のB細胞腫瘍治療

B細胞性リンパ腫とB細胞性慢性リンパ性白血病に対するベンダムスチンの有用性*

石澤賢一**

Key Words: bendamustine, chronic lymphocytic leukemia, indolent B-cell non-Hodgkin's lymphoma, mantle cell lymphoma, rituximab

はじめに

塩酸ベンダムスチンは構造的にアルキル化剤と代謝拮抗剤の特徴を有し，毒性が許容範囲内となるように設計された薬剤で，旧東ドイツのJenapharm社で合成され，1971年に旧東ドイツで販売が開始された．現在欧州ではドイツ，ブルガリアで低悪性度リンパ腫，慢性リンパ性白血病，骨髄腫を適応疾患として発売されている．米国では，2008年3月に慢性リンパ性白血病，同年10月にはリツキシマブ耐性低悪性度リンパ腫を適応として承認された．本邦でも，第I相試験，第II相試験が終了して，現在承認申請中である．

本剤はナイトロジェンマスタード基，プリン様ベンズイミダゾール基，酪酸側鎖の3つの部分で構成されている．ナイトロジェンマスタード基はcyclophosphamide, chlorambucil, melphalanと，酪酸側鎖はchlorambucilと共通である．またプリン様ベンズイミダゾール基は，プリン代謝拮抗剤のフルダラビン，クラドリビンと共通であり，これらを併せ持つユニークな構造は，既存の抗がん剤とは異なる作用機序が期待された[1]（図1）．事実，米国がん研究所のパネルスクリーニングによるコンペア解析では，cyclophosphamide, chlorambucil, melphalanでは相互に強い相関性が認められたが，これらのアルキル化剤と塩酸ベンダムスチンとの感受性の相関性は低く，既存のアルキル化剤とは異なる作用機序も有することが示唆された[2]．

これまで十分な質の高い臨床データが欠如していたこと，そのユニークな構造，作用機序より有効性，安全性の詳細な検討が必要であると考えられ，さまざまな条件下で臨床試験が実施された．

以下，低悪性度B細胞性リンパ腫，慢性リンパ性白血病に関して，その有効性，安全性を，主要な文献をもとに概説する．

低悪性度B細胞性リンパ腫に対する有効性，安全性

1．塩酸ベンダムスチン単剤の治療成績

(1)米国での第II相試験[3]

対象：再発，治療抵抗性低悪性度リンパ腫．単剤あるいは併用でのリツキシマブ投与歴があり，かつリツキシマブ抵抗性，あるいは不耐用と判断された症例．リツキシマブ抵抗性は，治療の反応しない，あるいは治療終了後6か月以内に病勢の進行を確認と定義された．

治療法：Day 1, 2 に塩酸ベンダムスチン120mg/m²を点滴静中．これを3週間ごとに病勢の進行が確認されない限り6コースを目標に，

* Efficacy of bendamustine in patients with chronic lymphocytic leukemia and B cell lymphoma.

** Kenichi ISHIZAWA, M.D., Ph.D.: 東北大学病院血液・免疫科〔〒980-8574 仙台市青葉区星陵町1-1〕; Department of Hematology & Rheumatology, Tohoku University Hospital, Sendai 980-8574, JAPAN

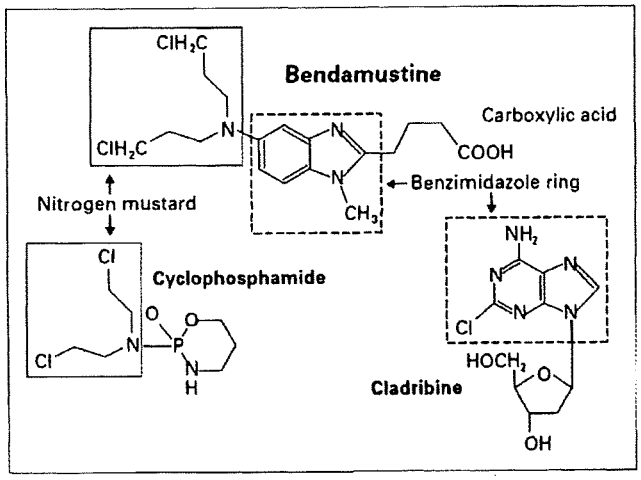

図1　塩酸ベンダムスチンの構造(文献[1]より引用改変)

治療効果が認められれば最大12コースまで投与するデザインで実施された.

症例数：期待全奏効率35%，閾値全奏効率20%として，目標症例数72症例.

結果：2003年9月から2005年2月まで，計77名が登録されたが1名が投与に至らず，解析対象は76名．年齢の中央値63歳(38～84歳)，前治療歴の中央値2レジメン(1～5レジメン)．組織学的進展例が15例含まれた.

実施コース数の中央値は5コース(1～9コース)で，目標の6コースを完遂できたのは34例(44%)であった．治療を6コース未満で中止した理由としては有害事象が23例で，そのうち血小板減少が最多で11例，原疾患の進行によるものが14例であった．放射免疫療法の治療歴がある9例中6例が血小板減少にて中止となり，減量が必要であったのは19例(25%)であった.

有害事象は血液毒性が主で，多くはグレード2以下が主であったが，グレード3以上の好中球減少が54%，血小板減少が25%認められた．非血液毒性では頻度順に悪心が72%，倦怠感が49%，嘔吐が41%認められたが，グレード3以上は倦怠感の7%が最多であった.

有効性は，全奏効率77%，完全寛解率34%．奏効持続期間の中央値は6.7か月で，組織型別の解析では，低悪性度リンパ腫で9.0か月，組織学的進展例で2.3か月．また観察期間の中央値26か月で，無増悪生存期間の中央値7.1か月．組織型別の解析では，低悪性度リンパ腫で8.3か月，組織学的進展例で4.2か月であった．アルキル化剤を含む化学療法で反応が認められなかった，あるいは増悪した23人の検討では，全奏効率61%で3例の完全寛解が確認された．またフルダラビン抵抗性8例の検討では，全奏効率は62%であった.

コメント：リツキシマブ抵抗例に対するベンダムスチンの有効性，安全性を前向きに評価した最初の試験である．高い奏効率が示され，有害事象も通常の支持療法で対応可能なレベルであり，単剤でも再発低悪性度リンパ腫治療において有力な選択肢となりうることが明らかになった．また少数例の検討ではあるが，アルキル化剤，プリン類似体抵抗例でも60%以上の全奏効率が得られており，米国でのコンペア解析の結果を*in vivo*で支持するものとなった．しかし低悪性度群と比較して，組織学的進展例での治療効果は明らかに劣っており，引き続き実施された第III相試験では対象から除外された.

(2)米国，カナダでの第III相試験[4]

対象：再発，治療抵抗性低悪性度リンパ腫で，組織学的進展例は除外し，1～3レジメンの化学療法の実施歴，単剤あるいは併用でのリツキシマブ投与歴があり，かつリツキシマブ抵抗性と判断された症例を対象とした．リツキシマブ抵

抗性は，リツキシマブ単剤4コース以上，リツキシマブ併用化学療法に反応しない，あるいは治療終了後6か月以内に病勢の進行，リツキシマブ維持療法中，終了6か月以内に病勢の進行が確認された症例と定義された．

治療法：Day 1, 2 に塩酸ベンダムスチン120mg/m²を点滴静中．これを3週間ごとに病勢の進行が確認されない限り，6～8コースを目標に投与するデザインで実施された．

症例数：期待全奏効率60%，閾値全奏効率40%として，目標症例数100症例．

結果：2005年10月から2007年7月まで，計102名が登録されたが2名投与に至らず，解析対象は100名．年齢の中央値60歳(31～84歳)，前化学療法歴の中央値2レジメン(0～6レジメン)．1例はリツキシマブ単剤のみで化学療法を受けておらず，8例は4レジメン以上の化学療法を受けていたため，プロトコル違反と判定されたが，解析対象とした．直近の化学療法に抵抗性であったのは36%．

実施コース数の中央値は6コース(1～8コース)で，目標の6コースを完遂できたのは60例(60%)．40例が治療6コース未満で中止となったが，その理由としては有害事象が27例(血小板減少9例，倦怠感6例など)，原疾患の進行によるものが10例．有害事象により減量が必要であったのは24%．全体では減量，投与延期，プロトコル中止となったのは68%であった．

有害事象は血液毒性が主で，グレード3以上の好中球減少が61%，血小板減少が25%，発熱性好中球減少は6%に認められた．非血液毒性は，悪心77%，感染症69%，倦怠感64%，下痢42%，嘔吐が40%認められた．グレード3以上が10%以上出現したものは，感染症21%，倦怠感14%であった．グレード4の感染症は6%であった．またCMV感染が5%認められた．過敏反応は14%認められた(表1)．

表1 ベンダムスチン単剤第III相試験の有害事象

有害事象	全グレード(%)	グレード3,4(%)
血液毒性		
貧血	94	10
血小板減少	88	25
好中球減少	83	61
発熱性好中球減少	6	6
非血液毒性		
悪心	77	4
感染	69	21
倦怠感	64	14
下痢	42	5
嘔吐	40	2
発熱	36	1
便秘	31	0

全グレードで20%以上． (文献[4]より引用改変)

有効性は，全奏効率75%，完全寛解率17%．病理組織別にみても，有効性に差はなかった(表2)．直近の化学療法に感受性あり(PR以上)の場合，全奏効率は88%，なしの場合は64%であった．またアルキル化剤を含む化学療法に感受性ありの場合，全奏効率は86%，なしの場合60%．治療奏効期間の中央値は9.2か月であった．また観察期間の中央値11.8か月で，無増悪生存期間の中央値7.5か月であった(図2)．アルキル化剤を含む化学療法に感受性ありの場合，無増悪生存期間の中央値は11.8か月，なしの場合7.5か月であった．

コメント：濃厚な治療歴を有する集団を対象に，全奏効率75%と，先に実施された第II相試験の結果が再現された．有効性に関しては本試験，安全性に関しては本試験と前述の第II相試験の結果を持って2008年10月，FDAはリツキシ

表2 ベンダムスチン単剤第III相試験の治療効果

	症例数	全奏効率(%)	CR+CRu(%)
全症例	100	75	17
病理組織別			
濾胞性リンパ腫	62	75	20
小リンパ球性リンパ腫	21	71	5
節性辺縁帯B細胞リンパ腫	9	78	11
節外性辺縁帯B細胞リンパ腫	7	86	43

(文献[4]より引用改変)

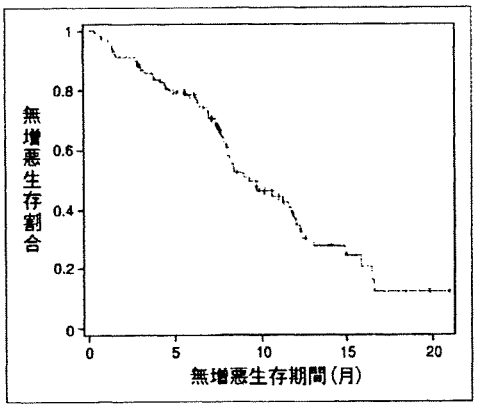

図2　ベンダムスチン単剤第III相試験の無増悪生存曲線　（文献[4]より引用改変）

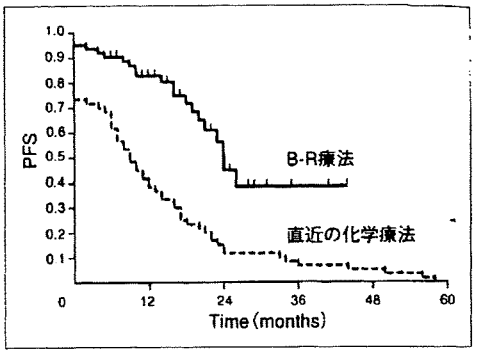

図3　B-R療法と直近の化学療法のPFSの比較　（文献[6]より引用改変）

マブ抵抗性の低悪性度B細胞性リンパ腫に対してベンダムスチンを承認した．

有害事象では，感染症が全グレードで69%，グレード3以上が21%と，これまでより高い頻度が報告された．注目されるのは，帯状疱疹12エピソード，CMV感染5エピソードと免疫抑制が強い可能性が示唆されたことである．原疾患，濃厚な治療歴の影響もあるが，ベンダムスチン投与後の免疫抑制に関しては，今後検討が必要な点である．

2．リツキシマブ併用の治療成績

ベンダムスチン単剤での高い有効性，動物モデルでリツキシマブ併用時に相乗効果が認められたことより[5]，リツキシマブとベンダムスチンの併用(B-R)療法が検討された．

(1)ドイツでの第II相試験[6]

対象：リツキシマブ未使用の，再発，治療抵抗性低悪性度リンパ腫，マントル細胞リンパ腫で，1~3レジメンの化学療法の既往がある症例．かつ，造血不全(Hb<11g/dlあるいは好中球<1,500/μlあるいは血小板数<10万/μl)，B症状の存在，リンパ腫関連症状のため治療が必要な症例．

治療法：Day 1にリツキシマブ375mg/m²，day 2, 3にベンダムスチン90mg/m²投与．これを4週間ごとに4コース繰り返し，1コース目の1週間前，4コース終了後4週間後にリツキシマブ375mg/m²を各1回投与するデザインで実施された．

結果：63名がエントリー．年齢の中央値64歳(40~81歳)．前治療歴1, 2, 3レジメンは，それぞれ43人，12人，8人．30%が直前の治療に抵抗性．マントル細胞リンパ腫16人中7人が前治療抵抗性．

63人中59人が予定の4コース完遂．2人が2コース(白血球減少1名，患者希望1名)，2人が3コース(1名が治療効果なし，1名が原因不明)で中止となった．

全奏効率90%，完全寛解率60%．マントル細胞リンパ腫に関しては，全奏効率75%，完全寛解率50%．PFSの中央値は24か月で，各症例の直前の治療後のPFSの中央値9か月より有意に(P<0.0001)延長していた(図3)．マントル細胞リンパ腫では，PFSの中央値が18か月で，解析時点で6名が最長22か月寛解を維持していた．全症例の48か月の時点でのOSは55%．

毒性に関しては血液毒性が中心で，グレード3(WHO)以上の白血球減少が16%認められたが，グレード3以上の血小板減少，貧血はそれぞれ3%，1%であった．非血液毒性は全般的に軽度で，悪心/嘔吐が43%に認められたが，グレード2以下であった．感染症に関しては，細菌性肺炎2例，帯状疱疹2例，口唇ヘルペスが2エピソード認められた．

コメント：リツキシマブとベンダムスチンの併用の最初の報告である．高い有効性が示され，リツキシマブを併用したにもかかわらず治療完遂率が高く，懸念された感染症が単剤より低頻

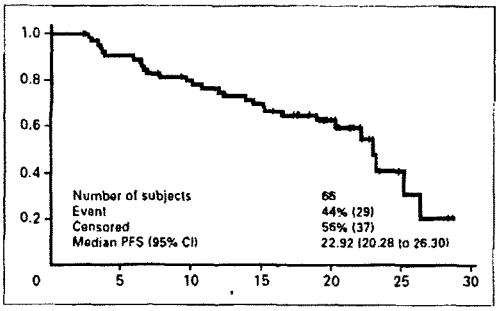

図4 米国第II相試験の無増悪生存曲線
(文献[7]より引用改変)

度であったことは，採用された投与法の妥当性を示したものである．またマントル細胞リンパ腫に関しても，少数例の検討ではあるが高い有効性が示され，その毒性がこれまでのマントル細胞リンパ腫で広く実施されているhyper-CVAD療法などと比較して軽度であることが注目される．

(2)米国の第II相試験[7]

対象：リツキシマブ抵抗性(リツキシマブを含む化学療法でPR未満，あるいは終了後6か月以内にPD)ではないCD20陽性再発低悪性度リンパ腫，マントル細胞リンパ腫．前治療は最大3レジメンまでで，放射免疫療法の既往がある症例は除く．

治療法：投与法はドイツの第II相試験と同様である．ただし腫瘍縮小が持続している場合は，最大6コースまで投与可能なデザインで実施された．

症例数：期待奏効率70%，閾値奏効率50%．検出力80%で症例数は60例．

結果：67名がエントリーしたが1名投与せず，解析対象は66名．年齢の中央値60歳(40～84歳)．前治療歴1,2,3レジメンは，それぞれ56%，33%，11%．リツキシマブの投与歴があるのは56%．アルキル化剤，プリンアナログ，アントラサイクリン系の使用歴はそれぞれ85%，23%，58%．

92%が4コース完遂．62%は6コースの投与を受けた．6例が4コース完遂できなかったが，その内訳は2例が有害事象，1例は原疾患の進行，2例が担当医の判断，1例が追跡不能のためであった．また計346サイクル実施され治療遅延12%であったが，そのうち74%は14日以内の遅延であった．Relative dose intensityの平均は，ベンダムスチン93%，リツキシマブ95%であった．

表3 リツキシマブ併用ベンダムスチン療法の治療効果

	ドイツの第II相試験	米国の第II相試験
全奏効率	90%	92%
CR率	60%	55%
PFS(中央値)	24か月	22.9か月

(文献[6][7]より引用改変)

全奏効率は92%，完全寛解率55%．観察期間の中央値が20か月で，治療奏効期間の中央値21か月，PFSの中央値が23か月(図4)．リツキシマブの投与歴の有無では，投与ありの場合，全奏効率87%，完全寛解率35%，投与なしの場合全奏効率100%，完全寛解率48%．マントル細胞リンパ腫12例に関しては，全奏効率92%，完全寛解率59%，治療奏効期間の中央値19か月であった．

有害事象は血液毒性が中心で，グレード3以上の好中球減少が36%，血小板減少が9%，貧血が2%認められた．非血液毒性では悪心70%，感染64%，倦怠感59%，便秘が44%認められたが大半はグレード2以下であった．グレード3以上は感染の10%が最多で，6例に10エピソード認められた．その内訳は，真菌感染2エピソード，ウイルス感染3エピソード，細菌感染，憩室炎，肺炎1エピソード，発熱性好中球減少2エピソードであった．グレード4のCMV感染が1エピソード認められた．

コメント：ドイツでの第II相試験で得られた高い治療効果(表3)と治療完遂率，単剤での第II相試験の結果と比較して低い感染症の頻度が再確認された試験である．

(3)ドイツでのB-R療法とR-CHOP療法の比較第III相試験[8]

対象：初発低悪性度リンパ腫，マントル細胞リンパ腫．

治療法：B-R療法(day 1 にリツキシマブ375mg/m^2，day 1,2 にベンダムスチン90mg/m^2)を28日ごと，または通常量のR-CHOP療法を21日

表4　B-R療法とCHOP-R療法の治療効果

	B-R療法	CHOP-R療法	
ORR	93.8%	93.5%	
CR率	40.1%	30.8%	$P=0.0323$
PFS(median)	54.8か月	34.8か月	$P=0.0002$
EFS	54か月	31か月	$P=0.0002$
TTNT	Not reached	40.7か月	$P=0.0002$

(文献[8]より引用改変)

ごとに最大6コース実施された.

患者背景：549名が登録．年齢の中央値は64歳(31～83歳)．組織型はB-R療法，R-CHOP療法それぞれ濾胞性リンパ腫55%，56%，マントル細胞リンパ腫18%，19%，他の低悪性度リンパ腫27%，24%.

結果：6コース完遂率はB-R療法82%，R-CHOP療法86%．全奏効率はB-R療法93.8%，R-CHOP療法63.5%．PFS, EFS, 次治療までの期間の中央値はB-R療法で54.8か月，54か月，中央値に達せず，R-CHOP療法で34.8か月，31か月，40.7か月と，いずれもB-R療法が上回った(表4)．

毒性に関しても，血液毒性ではグレード3以上の好中球減少はB-R療法で10.7%，R-CHOP療法で46.5%，グレード3以上の白血球減少がB-R療法で12.1%，R-CHOP療法で38.2%とB-R療法が軽度であった．非血液毒性に関しても脱毛，感染症，末梢神経障害，口内炎のいずれもB-R療法が軽度であった．薬剤関連の皮膚反応のみがB-R療法の方が高頻度であった.

コメント：現在低悪性度リンパ腫に対して広く実施されているR-CHOP療法とB-R療法のはじめての比較試験の結果である．有効性，安全性ともにB-R療法が上回っており，B-R療法が低悪性度リンパ腫初回治療の第一選択となる可能性を示唆したものとなった.

3．今後の検討課題

単剤投与での120mg/m² 2日間投与，1コース21日のスケジュールは，治療完遂率が低いこと，減量，遅延の頻度が高いこと，免疫抑制が強いことが推察され，一般臨床での使用では少し検討が必要と思われる.

また放射免疫療法実施の既往があると，血小板減少でベンダムスチン投与完遂が困難であることが示唆されたが，現在では放射免疫療法は再発早期の使用が推奨されているため，放射免疫療法との投与順序が今後問題となる．ベンダムスチン投与既往例における放射免疫療法実施後の血小板減少の程度も現時点で不明であり，ベンダムスチンのポジショニングに関しては，濾胞性リンパ腫の治療体系全体を考慮した検討が必要である.

マントル細胞リンパ腫に関しては，治癒を期待する強力な化学療法が実施できない症例，再発例に関しては，選択肢の1つとなるが，初回治療への組み込みに関しては今後の課題である.

慢性リンパ性白血病に対する有効性，安全性

1．塩酸ベンダムスチン単剤の治療成績

(1)再発例に対する第I/II相試験[9]

対象：クロラムブシルあるいはフルダラビンの治療歴のあるBinet B, C のCLL.

治療法：開始用量はベンダムスチン100mg/m²で，day 1, 2に投与して3～4週ごとに繰り返す．用量制限毒性(DLT)の有無により10mg/m²刻みで増量，減量するデザインで実施された．DLTはグレード3以上の非血液毒性，グレード4の原疾患によらない血液毒性と定義された.

結果：16名がエントリーされた．年齢の中央値は67歳(57～83歳)で，Binet C は10名．前治療レジメン数の中央値は3レジメン.

高尿酸血症，感染症，血液毒性などのDLTが複数100mg/m²，90mg/m²，80mg/m²コホートで観察され，MTD, 推奨用量ともに70mg/m²に決定された．奏効率(CR+PR+SD)56%でCR 2例であった.

コメント：非ホジキンリンパ腫と異なりCLLでは，原疾患により骨髄機能が低下していること，また免疫抑制状態にあり易感染性であることより用量の再検討が必要であり，結果的に再発非ホジキンリンパ腫に対する用量の約6割が推奨用量となった.

(2)初発例に対する第III相試験[10]

対象：未治療，CLL．Binet stage B, C.

治療法：ベンダムスチン投与群とクロラムブシル投与群に1：1に無作為化割り付け．ベンダムスチンは100mg/m²をday 1, 2に投与．1コー

スを4週間として，治療効果により最大6コースまで投与．クロラムブシル群は0.8mg/kgをday 1, 15に投与．1コースを4週間として，同様に治療効果により最大6コースまで投与．

結果：ベンダムスチン群162例，クロラムブシル群157例の計319例が登録．Binet stage B, Cの割合は，ベンダムスチン群71.6%，28.4%．クロラムブシル群70.7%，29.3%．

全奏効率はベンダムスチン群68%(CR率31%)，クロラムブシル群31%(CR率2%)．無増悪生存率の中央値はベンダムスチン群21.6か月，クロラムブシル群8.3か月(図5)．

有害事象の頻度はベンダムスチン群89%，クロラムブシル79%．一般的なものは，好中球減少，発熱，血小板減少，悪心，貧血，白血球減少，嘔吐などで，ベンダムスチン群では9例が過敏反応で治療中止となった．

コメント：ベンダムスチンの有効性はクロラムブシルを上回り，その毒性は管理可能であること，またこれまでのフルダラビン単剤の報告に匹敵する有効性が示された．本試験の結果をもってFDAは2008年3月，CLLに対してベンダムスチンを承認した．

2．リツキシマブ併用の治療成績：初発CLLに対する第II相試験[11]

対象：治療を要する初発CLL．

治療法：ベンダムスチン90mg/m²をday 1, 2に投与し，28日ごとに最大6コース実施．リツキシマブは1コース目は375mg/m²，2コース目以降は500mg/m²投与．

結果：117名がエントリーされ，合計583コース実施された．Binet A, B, Cは，それぞれ11.1%，41.0%，47.9%．全奏効率90.9%，CR率32.7%．主な有害事象は骨髄抑制で，グレード3以上の頻度は，全実施コース数あたり貧血4.9%，白血球減少14.6%，好中球減少6.5%，血小板減少6.1%．グレード3以上の感染症は29エピソード，全実施コース数の5.1%に認められた．

コメント：B-R療法の未治療CLLの有効性を明らかにしたもので，有害事象も懸念された感染症を含めて許容範囲であった．この結果を受けてドイツではB-R療法とFCR療法の比較試験を実施中である．

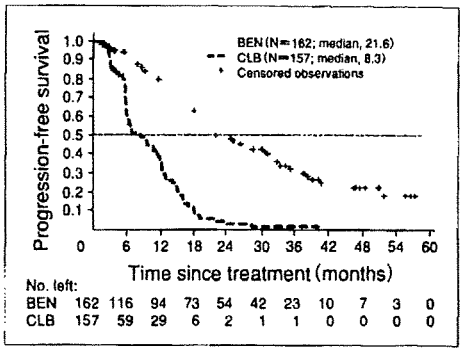

図5 クロラムブシル，ベンダムスチン群の無増悪生存曲線 (文献[10]より引用改変)

3．今後の検討課題

これまでの試験の成績をみる限り，既治療例に対してベンダムスチンが治療選択肢の1つとなるのは明らかである．初発例に関しては，第III相試験はクロラムブシルとの比較である点が議論を呼ぶところであり，B-R療法とFCR療法の比較試験の結果が待たれる．

文　献

1) Cheson BD, Rummel MJ. Bendamustine : rebirth of an old drug. J Clin Oncol 2009 ; 27 : 1492.
2) Leoni LM, Bailey B, Reifert J, et al. Bendamustine (Treanda) displays a distinct pattern of cytotoxicity and unique mechanistic features compared with other alkylating agents. Clin Cancer Res 2008 ; 14 : 309.
3) Friedberg JW, Cohen P, Chen L, et al. Bendamustine in patients with rituximab-refractory indolent and transformed non-Hodgkin's lymphoma : results from a phase II multicenter, single-agent study. J Clin Oncol 2008 ; 26 : 204.
4) Kahl BS, Bartlett NL, Leonard JP, et al. Bendamustine is effective therapy in patients with rituximab-refractory, indolent B-cell non-Hodgkin's lymphoma. Cancer 2009 (published online).
5) Chow KW, Sommerlad WD, Boehrer S, et al. Anti-CD20 antibody (IDEC-C2B8, rituximab) enhances efficacy of cytotoxic drugs on neoplastic lymphocyte in vitro : role of cytokines, complement, and caspases. Haematologica 2002 ; 87 : 33.

6) Rummel MJ, Al-Batran SE, Kim SZ, et al. Bendamustine plus rituximab is effective and has a favorable toxicity profile in the treatment of mantle cell and low-grade non-Hodgkin's lymphoma. J Clin Oncol 2005 ; 23 : 3383.
7) Robinson KS, Williams ME, van der Jart RH, et al. Phase II multicenter study of bendamustine plus rituximab in patients with relapsed indolent B-cell and mantle cell non-Hodgkin's lymphoma. J Clin Oncol 2008 ; 26 : 1.
8) Remmel MJ, Niederle N, Maschmeyer G, et al. Bendamustine plu rituximab is superior in respect of progression free survival and CR rate when cpmpared to CHOP plus rituximab as front-line treatment of patients with advanced follicular, indolent, and mantle cell lymphoma : final results of a randomized phase III study of the Stil (Study Group Indolent Lymphoma, Germany). Blood 2009 ; 114 : abstr405.
9) Bergmann MA, Goebeler ME, Herold M, et al. Efficacy of bendamustine in patients with relapsed or refractory chronic lymphocytic leukemia : results of a phase I/II stuidy of the German CLL Study Group. Haematologica 2005 ; 90 : 1357.
10) Knauf WU, Lissichkov T, Aldaoud A, et al. Phase-III randomized study of bendamustine compared with chlorambucil in previously untreated patients with chronic lymphocytic leukemia. J Clin Oncol 2009 ; 27 : 4378.
11) Fisher K, Cramer P, Stilgenbauer S, et al. Bendamustine combined with rituximab (BR) in first-line therapy of advanced CLL : a multicenter phase II trial of the German CLL Study Group (GCLLSG). Blood 2009 ; 114 : abstr205.

* * *

Biochemical and Biophysical Research Communications 390 (2009) 48–53

Contents lists available at ScienceDirect

Biochemical and Biophysical Research Communications

journal homepage: www.elsevier.com/locate/ybbrc

Escape mechanisms from antibody therapy to lymphoma cells: Downregulation of *CD20* mRNA by recruitment of the HDAC complex and not by DNA methylation

Takumi Sugimoto [a], Akihiro Tomita [a,*], Junji Hiraga [a,b], Kazuyuki Shimada [a], Hitoshi Kiyoi [c], Tomohiro Kinoshita [a], Tomoki Naoe [a]

[a] *Department of Hematology and Oncology, Nagoya University Graduate School of Medicine, Nagoya, Japan*
[b] *Department of Hematology, Toyota Memorial Hospital, Toyota, Japan*
[c] *Department of Infectious Diseases, Nagoya University School of Medicine, Nagoya, Japan*

ARTICLE INFO

Article history:
Received 15 September 2009
Available online 19 September 2009

Keywords:
CD20
Rituximab
Epigenetics
Histone deacetylases
DNA methytransferases

ABSTRACT

Although rituximab is a critical monoclonal antibody therapy for CD20-positive B-cell lymphomas, rituximab resistance showing a CD20-negative phenotypic change has been a considerable clinical problem. Here we demonstrate that *CD20* mRNA and protein expression is repressed by recruitment of a histone deacetylase protein complex to the *MS4A1* (*CD20*) gene promoter in CD20-negative transformed cells after treatment with rituximab. *CD20* mRNA and protein expression were stimulated by decitabine (5-Aza-dC) in CD20-negative transformed cells, and was enhanced by trichostation A (TSA). Immunoblotting indicated that DNMT1 expression was first downregulated 1 day after treatment with 5-Aza-dC, but IRF4 and Pu.1, the transcriptional regulators of *MS4A1*, were still expressed with or without 5-Aza-dC. Interestingly, CpG methylation of the *MS4A1* promoter was not observed in CD20-negative transformed cells without 5-Aza-dC. A chromatin immunoprecipitation (ChIP) assay indicated that the Sin3A–HDAC1 co-repressor complex was recruited to the promoter and dissociated from the promoter with 5-Aza-dC and TSA, resulting in histone acetylation. Under these conditions, IRF4 and Pu.1 were continually recruited to the promoter with or without 5-Aza-dC and TSA. These results suggest that recruitment of the Sin3A–HDAC1 complex is related to downregulation of CD20 expression in CD20-negative B-cells after treatment with rituximab.

Introduction

Rituximab is the first therapeutic monoclonal antibody targeting human malignant tumors, and is now an indispensable molecular-targeting drug for CD20-positive B-cell lymphomas [1–3]. Although the effectiveness is significant, resistance to rituximab has also become a considerable problem [4].

Several mechanisms of the resistance have been suggested, including loss of CD20 protein expression after rituximab use [5–12] and CD20 gene mutations [13]. Furthermore, other mechanisms have also been suggested [4] such as internalization of CD20 protein [14], interference with accessibility of rituximab to CD20 protein by inhibitory factors, rapid metabolism of the antibody, abnormalities in B-cell signaling in tumor cells [15], abnormalities of apoptosis [16], antibody-dependent cell-mediated cytotoxicity (ADCC), and complement-dependent cytotoxicity (CDC) [17].

Very recently, we reported observation of downregulation of CD20 protein expression in CD20-positive B-cell lymphoma patients after treatment with rituximab-containing combination chemotherapies [6,7]. In those cases, it was strongly suggested that aberrant downregulation of *MS4A1* expression was closely related to the loss of CD20 protein expression, and that expression of CD20 and rituximab sensitivity were partially restored by some molecular-targeting drugs [6,7]. Although these findings suggest that epigenetic mechanisms, in part, contribute to the downregulation of CD20 expression, the molecular mechanisms are still not clear. Furthermore, a recent report indicated that reduced CD20 protein expression in *de novo* diffuse large B-cell lymphoma is associated with a poor survival rate [18]. Thus, understanding the mechanisms of downmodulation of CD20 protein expression is likely to be very important from both basic research and clinical viewpoints.

In this report, we show that the recruitment of a histone deacetylase (HDAC) co-repressor complex to the *MS4A1* promoter

* Corresponding author. Address: Department of Hematology and Oncology, Nagoya University Graduate School of Medicine, Tsurumai-Cho 65, Showa-ku, Nagoya 466-8560, Japan. Fax: +81 52 744 2161.
E-mail address: atomita@med.nagoya-u.ac.jp (A. Tomita).

0006-291X/$ - see front matter © 2009 Elsevier Inc. All rights reserved.
doi:10.1016/j.bbrc.2009.09.059

region, but not DNA methylation [19], is involved in CD20-negative phenotypic changes in B-cell lymphoma cells after treatment with rituximab. We show that the complex dissociated from the promoter in the presence of a DNA methyltransferase (DNMT) inhibitor and a HDAC inhibitor [20], resulting in partial restoration of CD20 expression.

Materials and methods

Cell culture conditions and treatment with epigenetic drugs. RRBL1 [6], Raji, and NALM6 cells were cultured in RPMI 1640 medium (Sigma–Aldrich, St. Louis, MO, USA) with 10% fetal calf serum. Five-Aza-dC (5-aza-2′-deoxycytidine; Sigma, St. Louis, MO) and TSA (Sigma) at final concentrations of 100 μM and 100 nM, respectively, were added directly to the culture medium.

Immunoblotting. Cells ($\sim 5 \times 10^5$) were lysed in 100 μl of lysis buffer (50 mM Tris–HCl, pH 8.0, 1.5 mM $MgCl_2$, 1 mM EGTA, 5 mM KCl, 10% glycerol, 0.5% NP-40, 300 mM NaCl, 0.2 mM PMSF, 1 mM DTT, and a complete mini protease inhibitor tablet (Roche)). After centrifugation at 10,000 *g* for 10 min, the supernatants were placed in new tubes, and 100 μl of 2× SDS sample buffer was added. After boiling for 5 min, samples were separated with SDS–polyacrylamide gel electrophoresis (SDS–PAGE). Immunoblotting was carried out as described previously [21,22] using anti-CD20, -IRF4, -Pu.1, -GAPDH antibodies (Santa Cruz Biotechnology, Santa Cruz, CA, USA), and anti-DNMT1 antibody (Abcam, Cambridge, MA, USA).

RNA preparation and reverse transcriptase-polymerase chain reaction (RT-PCR). RNA from cell lines (1×10^5 cells) was obtained using Trizol (Invitrogen, Carlsbad, CA, USA). Complementary DNA (cDNA) was prepared as reported previously [7,22].

For RT-PCR, the following primers were designed: CD20-U; 5′-ATGAAAGGCCCTATTGCTATG-3′, CD20-L; 5′-GCTGGTTCACAGTTGTATATG-3′, β-actin-U; 5′-TCACTCATGAAGATCCTCA-3′, and β-actin-L; 5′-TTCGTGGATGCCACAGGAC-3′. Semi-quantitative RT-PCR with AmpliTaq Gold was performed as described previously [6].

Methylation status of the MS4A1 promoter. To examine the methylation status, bisulfite sequencing was performed. Genomic DNA was prepared with a QIAamp DNA Blood Mini kit (Qiagen, Valencia, CA, USA). Bisulfite treatment was performed using EpiTect Bisulfite kits (Qiagen). After bisulfite treatment, PCR of the *MS4A1* promoter was performed using the specific primers as follows, MS4A1-pro-MSPU; 5′-GGTAGTATGAGTATGTTAGGTAGTT-3′, MS4A1-pro-MSPL; 5′-TTTTCCTTACCTAAATCTCCAAAA-3′. PCR fragments were cloned into a pGEM-T easy vector (Promega, Madison, WI, USA) and sequenced.

Flow cytometry (FCM) analysis. Cell surface antigens of RRBL1 with or without 5-Aza-dC and TSA treatment were analyzed using a BD FACSCalibur Flow Cytometer (BD Bioscience, Franklin Lakes, NJ, USA) with anti-CD20 antibody (Leu-16 PE, BD) and mouse IgG1 κ isotype control (PE-Cy7, BD).

Chromatin immunoprecipitation (ChIP) assay. The ChIP assay was performed as described previously [22,23]. For immunoprecipitation (IP), the following antibodies were used; anti-Pu.1, -IRF4 (Santa Cruz Biotechnology), -acetylated H4 (Millipore, Billerica, MA, USA), -Sin3A, and anti-HDAC1 (Abcam) antibodies. Immunoprecipitated DNA was used for semi-quantitative PCR using LA-Taq polymerase (TAKARA, Ohtsu, Japan). The following primers for the *MS4A1* promoter and 3′-intron sequence (negative control) were used; CD20pro-U; 5′-CTAAAAGTGAAGCCAGAAGG-3′, CD20pro-L; 5′-GGAGGGTGAGTGGTGTAGT-3′, CD20-3′U; 5′-GCTGACCTCACATAACTCCT-3′, CD20-3′L; 5′-GAAATCCCTCAGACTCAGAC-3′.

Immunoprecipitation (IP) assay. The IP assay was carried out as described previously [22]. Whole cell lysate was obtained from RRBL1 cells (1×10^7) using 800 μl of lysis buffer. After adding 800 μl of lysis buffer without NP-40 and NaCl, the lysate was divided into four tubes (400 μl each) and IP using anti-IRF4, -Sin3A, and -HDAC1 antibodies was performed. The precipitated samples were applied to SDS–PAGE followed by immunoblotting. For the pre-IP samples, 5% of the whole cell lysate was used.

Results

CD20 protein and mRNA expression were stimulated by treatment with 5-Aza-dC in CD20-negative transformed cells

As we reported previously [6,7], the downregulation of CD20 protein and mRNA expression has been observed in some CD20-positive B-cell lymphoma patients after treatment with rituximab-containing chemotherapies. We also reported that the downregulation of CD20 expression was partially stimulated by treatment with the epigenetic drugs 5-Aza-dC and TSA. RRBL1 cells were established from a patient with B-cell lymphoma who showed a CD20-negative phenotypic change after treatment with rituximab [6]. To examine the mechanisms of stimulation of CD20 expression by 5-Aza-dC, we examined the protein expression pattern that may affect CD20 gene transcription in RRBL1 cells. RRBL1 cells were treated with 5-Aza-dC for 24 h, and were then washed and incubated for up to 7 days (Fig. 1A). During this procedure, the cells were harvested several times as indicated and analyzed using semi-quantitative RT-PCR and immunoblotting (IB) (Fig. 1B). *CD20* mRNA and protein expression were stimulated by 5-Aza-dC, and the peak of expression was observed around day 3 after treatment with 5-Aza-dC (lane 6). After day 5, CD20 protein expression had gradually decreased. DNMT1 depletion was confirmed at 24 h after treatment with 5-Aza-dC (lane 4) as reported previously [24]. IRF4 and Pu.1 are transcription factors that interact with the *MS4A1* promoter and regulate CD20 expression [25]. IRF4/Pu.1 was almost constantly expressed throughout the 5-Aza-dC treatment duration (lanes 3–8), but only a modest upregulation was observed after treatment with 5-Aza-dC around day 2 (lane 5). These results suggested that DNMT1 depletion by 5-Aza-dC may be related to stimulation of *MS4A1* expression.

DNA methylation status of the MS4A1 promoter

To explain the activation of *CD20* mRNA and protein expression after treatment with 5-Aza-dC in RRBL1 cells, we next examined the CpG methylation status of the *MS4A1* promoter (Fig. 1C). Interestingly, CpG islands were not observed on the promoter region located ~5 kb upstream from the transcription start site, and only four CG sites were found on the promoter from the −1000 to +100 region. Bisulfite sequencing was carried out to confirm methylated CpG. As shown in Fig. 1C, no CpG methylation was observed on the three CpG sites around the transcription start site in RRBL1 cells. In NALM6 cells, a CD20-negative lymphoblastic leukemia cell line, several methylated CpGs were observed. Furthermore, the same analysis was performed using primary tumor cells from a patient suffering from CD20-negative transformed B-cell lymphoma after treatment with rituximab-containing combination chemotherapies. (Detailed information about this patient is described in our previous paper as UPN3 [7]). The three CpG sites were not methylated, as observed in RRBL1 cells (Fig. 1C, UPN3). These results suggest that transcriptional activation of *MS4A1* by 5-Aza-dC may not be regulated by its promoter CpG demethylation in RRBL1 cells.

Histone deacetylase inhibitor TSA enhances CD20 expression by 5-Aza-dC in CD20-negative transformed cells

Next, we analyzed the effect of a HDAC inhibitor in addition to 5-Aza-dC on *MS4A1* expression in RRBL1 cells. CD20 protein expression in RRBL1 cells was confirmed using immunoblotting

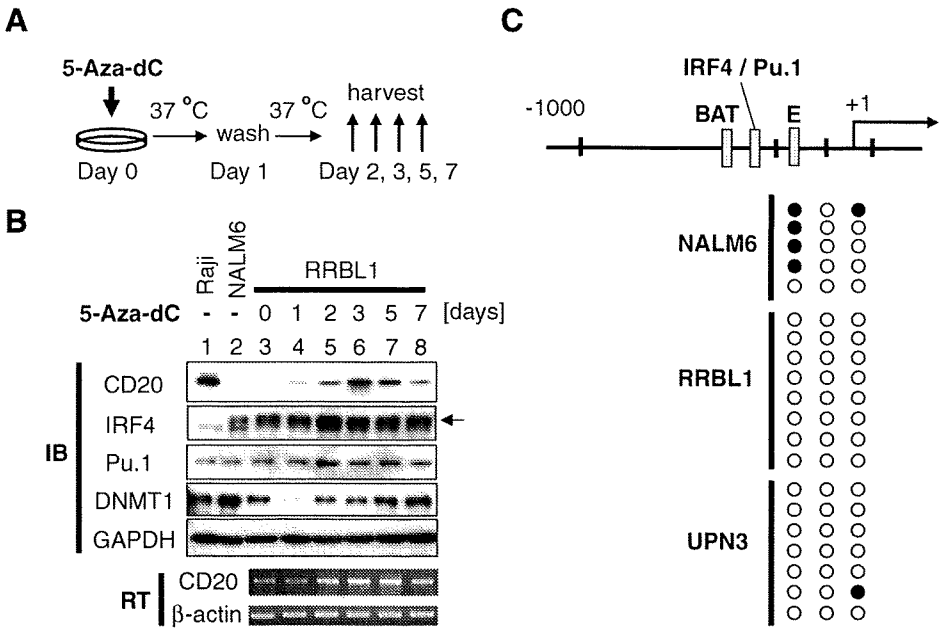

Fig. 1. CD20 protein and mRNA expression were transiently stimulated by treatment with a DNMT inhibitor. (A) Schematic representation of 5-Aza-dC treatment of the CD20-negative transformed B-lymphoma cells. RRBL1 cells were incubated at 37 °C for 24 h, and then washed twice with RPMI medium with 10% FCS without 5-Aza-dC. Cells were further incubated for up to 7 days, and were harvested at days 1, 2, 3, 5, and 7. (B) Protein expression was examined using immunoblotting (IB) with the indicated antibodies. The mRNA expression level was determined using semi-quantitative RT-PCR (RT). The black arrow indicates the band for IRF4. Raji and NALM6 cells were used as positive and negative controls, respectively. GAPDH and β-actin were measured as internal controls. (C) The structure of the *MS4A1* promoter near the transcription start site (from −1000 to +100) is depicted. The BAT-box, IRF4/Pu.1 binding sites, and E-box are shown as shaded boxes. Only four CpG sites, which are putative methylation sites, were found and are shown as black vertical bars. The methylation status of the three CpG sites around the transcription start site in NALM6, RRBL1, and primary B-lymphoma cells that show CD20-negative transformation was analyzed with bisulfite sequencing. Five to eight clones were analyzed from each sample. Black and open circles indicate methylated and non-methylated CpGs, respectively.

and flow cytometry (FCM) (Fig. 2A and B) following treatment with 5-Aza-dC and/or TSA. When RRBL1 cells were treated with 5-Aza-dC or TSA alone, minimal activation of CD20 protein expression was observed using immunoblotting (Fig. 2A, lanes 4 and 5) and FCM (Fig. 2B, 5-Aza-dC). In the presence of 5-Aza-dC and TSA, CD20 protein expression was significantly increased (Fig. 2A, lane 6, and B, 5-Aza-dC + TSA). These results suggested that *MS4A1* expression is, in part, regulated by epigenetic mechanisms such as histone modification including lysine acetylation, rather than DNA CpG methylation of the *MS4A1* promoter.

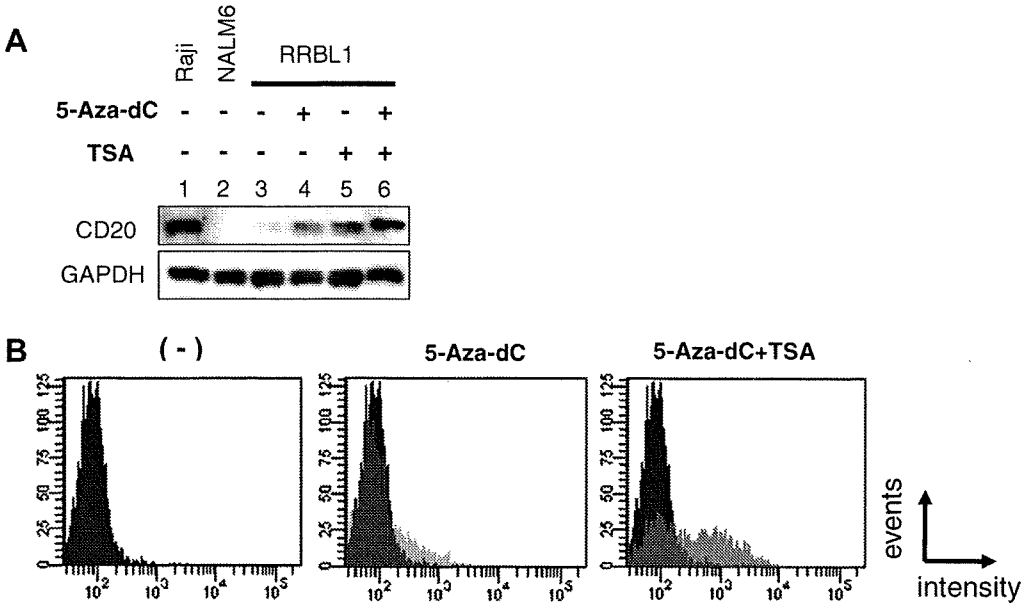

Fig. 2. CD20 protein expression by 5-Aza-dC was enhanced by TSA. CD20 protein expression was shown with IB (A) and FCM (B) with or without epigenetic drugs. For 5-Aza-dC treatment, RRBL1 cells were incubated with 5-Aza-dC for 24 h followed by washing and two additional days of incubation. TSA was added at the start of day 3, and cells were incubated for 24 h. If cells were not treated with 5-Aza-dC, washing was also carried out at day 1 to adjust the incubation conditions. All the cells were harvested at day 4 and utilized for IB and FCM analyses. The untreated and treated cells with the epigenetic drugs were depicted as black and gray areas, respectively (B).

Recruitment of co-repressor proteins and histone deacetylation on the MS4A1 promoter in the absence of epigenetic drugs

To study the molecular mechanisms of transcriptional repression of *MS4A1*, a ChIP assay was performed. RRBL1 cells were incubated with or without 5-Aza-dC and TSA, and a ChIP assay was carried out using anti-Pu.1, -IRF4, -Sin3A, -HDAC1, and -acetylated-histone H4 antibodies. After IP, precipitated genomic DNA was utilized in semi-quantitative PCR using primers for the *MS4A1* promoter (Fig. 3A) and the 3′-intron sequences as a negative control. IRF4 and Pu.1 interactions were consistently observed on the promoter region, but not on the 3′-intron region (Fig. 3B, lanes 5–8). Sin3A and HDAC1, which form a transcription repressor protein complex [26], interacted with the promoter region only in the absence of 5-Aza-dC and TSA (Fig. 3B, lanes 11 and 13). Acetylated-histone H4 was observed at the promoter region with 5-Aza-dC and TSA, but the acetylation was decreased in the absence of the two drugs (lane 9). In the 3′-intron region, histone acetylation was consistently observed with or without 5-Aza-dC and TSA. These results strongly suggest that the Sin3A–HDAC1 co-repressor complex may be recruited to the *MS4A1* promoter through some transcription factors in the absence of epigenetic drugs, resulting in histone deacetylation and transcriptional repression. In addition, the recruitment may be dissociated from the promoter by adding 5-Aza-dC and TSA, resulting in histone acetylation and transcription activation.

The Sin3A–HDAC1 co-repressor complex is found in RRBL1 cells with or without epigenetic drugs

To show that loss of Sin3A–HDAC1 interaction with the *MS4A1* promoter was due to protein complex dissociation and not degradation, we confirmed the protein expression in RRBL1 cells with and without epigenetic drugs using IB. As shown in Fig. 4A, HDAC1 and Sin3A protein expression levels did not change in the presence of epigenetic drugs. Next, we performed an IP assay using anti-IRF4, -Sin3A, and -HDAC1 antibody to confirm that Sin3A and HDAC1 exist as a protein complex, and to examine whether the Sin3A–HDAC1 co-repressor complex was recruited by IRF4 in the absence of epigenetic drugs. The Sin3A–HDAC1 interaction was confirmed with an IP assay using anti-Sin3A and -HDAC1 antibodies (Fig. 4B, lanes 4 and 5), but interaction of IRF4 with this complex was not observed (lane 3). These results indicate that the Sin3A–HDAC1 complex exists in RRBL1 cells with or without 5-Aza-dC and TSA, and that the recruitment of the complex to the *MS4A1* promoter may not involve a direct interaction with IRF4.

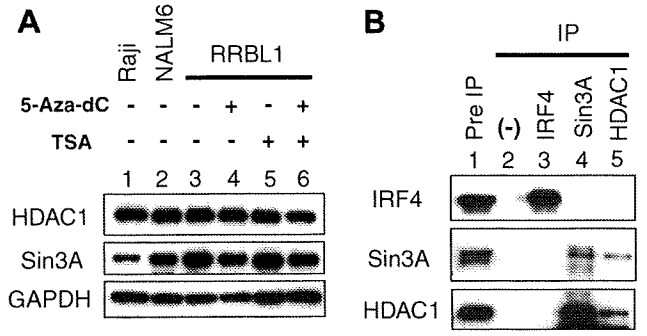

Fig. 4. The Sin3A–HDAC1 co-repressor complex is stably expressed in RRBL1 cells with or without 5-Aza-dC and/or TSA. (A) IB was performed using the RRBL1 lysate after treatment with 5-Aza-dC and/or TSA. Raji and NALM6 cells were used as expression controls. Similar levels of expression of HDAC1 and Sin3A were observed in each sample. (B) Whole cell lysate of RRBL1 cells was obtained using lysis buffer. Lysates were divided into four samples and used for IP using anti-IRF4, -Sin3A, and -HDAC1 antibodies. Five percent of the whole cell lysate was used for the pre-IP samples (lane 1). As a negative control, antibodies for IP were omitted (lane 2). IB indicated that endogenous Sin3A–HDAC1 interacted in RRBL1 cells without epigenetic drugs, but significant interaction with IRF4 was not observed in this assay system.

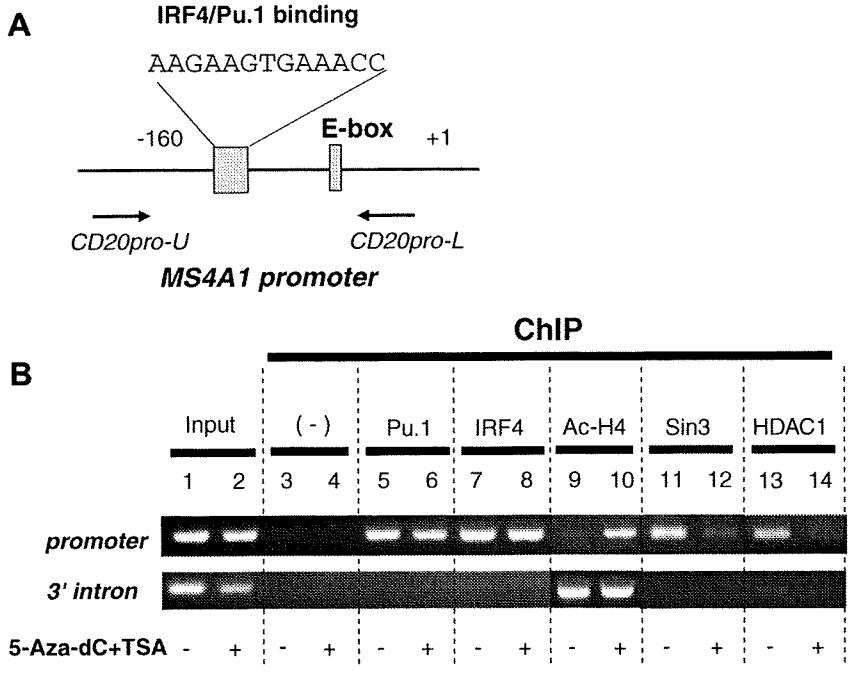

Fig. 3. ChIP assay of the *MS4A1* promoter. The primer set used for amplification of the *MS4A1* promoter (−160 to +1) is shown in (A). The positions of the upper and lower primers are indicated as black arrows. (B) A ChIP assay using anti-Pu.1, -IRF4, -Sin3A, -HDAC1, and -acetylated-histone H4 was performed using the cell lysate from cells treated with or without 5-Aza-dC and TSA. Semi-quantitative PCR was performed, and the amplified DNA fragments were visualized by 1.5% agarose gel electrophoresis. As a positive control, lysate without the IP step was used (input). A ChIP sample without antibodies was used as a negative control (−). PCR using the primers for the 3′-intron region of *MS4A1* was also used as a control. Sin3A and HDAC1 recruitment to the promoter was observed in lanes 11 and 13, and accumulation of histone deacetylation was seen in lane 9.